Available online at www.sciencedirect.com
SCIENCE DIRECT®
International Journal of Heat and Fluid Flow 26 (2005) 141–155
International Journal of HEAT AND FLUID FLOW
www.elsevier.com/locate/ijhff

A mixture theory model for the forced convection flow through an unsaturated wellbore

Maria Laura Martins-Costa [a,*], Rogério M. Saldanha da Gama [b]

[a] Laboratory of Theoretical and Applied Mechanics, Department of Mechanical Engineering, Universidade Federal Fluminense, Rua Passo da Pátria, 156, Niteroi, RJ, 24210-240, Brazil
[b] Department of Mechanical Engineering, Universidade do Estado do Rio de Janeiro, Rua São Francisco Xavier 524, 20550-013, Brazil

Received 17 July 2003; accepted 6 June 2004
Available online 27 August 2004

Abstract

This work studies the dynamics of the filling up of a rigid cylindrical porous matrix by a Newtonian fluid and the heat transfer associated phenomenon. A mixture theory approach is employed to obtain a preliminary local description for non-isothermal flows through a wellbore. The mixture consists of three overlapping continuous constituents, representing the porous matrix (solid constituent), the Newtonian fluid (liquid constituent) and an inert gas included to account for the compressibility of the mixture as a whole. Assuming the convective flow on radial direction only, a set of four non-linear partial differential equations describes the problem. Its hydrodynamic part—a non-linear hyperbolic system—is approximated by means of a Glimm's scheme, combined with an operator splitting technique, while an implicit finite difference scheme is used to simulate the thermal part. Some examples illustrate the proposed strategy.

Keywords: Unsaturated porous medium; Forced convection; Mixture theory; Riemann problem; Shock waves; Operator splitting

1. Introduction

Among the practical applications of transport phenomena in porous media, groundwater flows, enhanced oil recovery processes, contamination of soils by hazardous wastes, storage of nuclear waste material in deep earth rock layers or deep ocean sea beds and pollution movement, could be mentioned. The increasing interest related to such phenomena may be explained by the importance attached to problems that impact the energy self-sufficiency and the environmental state.

Transport phenomena in unsaturated porous media are characterized by a strong dependence of the motion on the saturation. Since the media are partially saturated, there is a force (depending on the saturation gradient) giving rise to a fluid flow. According to Tien and Vafai (1990), these phenomena have been studied since the 1920s, emphasizing momentum transport. The drying phenomenon was simulated supposing that the fluid motion through the porous medium was caused by diffusion only (the balance of linear momentum was substituted by the diffusion equation). In other studies the influence of capillary forces (surface tension) in the modeling of liquid motion has also been considered.

This work studies the dynamics of the filling up of a rigid cylindrical shell porous matrix by a Newtonian fluid and the heat transfer associated phenomenon, in order to build a preliminary local description for non-isothermal flows through a wellbore, using a mixture theory approach in the mechanical modeling. This method of attack a convenient one for modeling multicomponent

* Corresponding author. Tel.: +55 21 2620 7070; fax: +55 21 2717 4446.
E-mail addresses: laura@mec.uff.br (M.L. Martins-Costa), rsgama@domain.com.br (R.M. Saldanha da Gama).

0142-727X/$ - see front matter © 2004 Elsevier Inc. All rights reserved.
doi:10.1016/j.ijheatfluidflow.2004.06.003

Nomenclature

A_F	dimensionless diffusive term coefficient—fluid constituent equation
A_S	dimensionless diffusive term coefficient—solid constituent equation
B_F	dimensionless internal source term coefficient—fluid constituent equation
B_S	dimensionless internal source term coefficient—solid constituent equation
c_f	fluid specific heat—measured in a Continuum Mechanics context
c_s	solid specific heat—measured in a Continuum Mechanics context
D	diffusion coefficient
k_f	fluid thermal conductivity—Continuum Mechanics context
k_s	porous matrix thermal conductivity—Continuum Mechanics context
K	porous matrix specific permeability
$\mathbf{m}_F$	momentum supply acting on the fluid constituent
p_0	reference pressure
$\mathbf{q}_F$	partial heat flux associated with the fluid constituent
$\mathbf{q}_S$	partial heat flux associated with the solid constituent
R_{FS}	internal heat source coefficient
T_F	fluid constituent temperature
T_S	solid constituent temperature
u	fluid constituent dimensionless velocity
$\mathbf{v}_F$	fluid constituent velocity
γ	dimensionless Darcian term coefficient
ε	porous matrix porosity
λ	associated eigenvalue
$\lvert\lambda\rvert_{max}$	maximum absolute value among all eigenvalues
Λ	parameter depending on the porous medium thermal properties and internal structure
μ_f	fluid viscosity—measured in a Continuum Mechanics context
Π_F	internal heat source associated with the fluid constituent
Π_S	internal heat source associated with the solid constituent
θ_F	dimensionless fluid constituent temperature
θ_S	dimensionless solid constituent temperature
ρ_F	fluid constituent mass density
ρ_f	actual mass density of the fluid—regarded as a single continuum
τ	dimensionless time
ξ	dimensionless position
ψ	saturation

systems was first presented within the framework of Continuum Mechanics by Truesdell (1957). A detailed development of the conservation laws, along with a discussion on their thermodynamic consistency is presented in this work (Truesdell, 1957). Its basic assumption is that, at any time, all the constituents are present at every point of the mixture. This method is a convenient one for treating multicomponent systems—being supported by a local theory with thermodynamic consistency which generalizes the classical Continuum Mechanics (Germain and Muller, 1986; Gurtin, 1981). The unsaturated porous medium is modeled as a mixture of three overlapping continuous constituents: a solid (a rigid, homogeneous and isotropic porous matrix), a liquid (an incompressible Newtonian fluid) and an inert gas, assumed with zero mass density; which was included to account for the compressibility of the system as a whole.

Among the approaches usually employed for dealing with transport phenomena in porous media, the most widely used is the volume averaging technique. In this approach, concentration and velocity components are described as volumetric averages in order that the momentum transport may be described in a classical continuum mechanics context. This approach has already allowed the analysis of complex problems, among which one could mention, for instance, the multiphase transport process with phase change in unsaturated porous media (Vafai and Whitaker, 1986), or the mixed convection (Aldouss et al., 1996; Chang and Chang, 1996; Chen et al., 1996). A comparison among different models for transport in porous media employing a volume averaging approach is found in Alazmi and Vafai (2000).

Among the relevant works employing a volume averaging approach those due to Amiri and Vafai (1994) and Sozen and Vafai (1990) worth mentioning. The former (Amiri and Vafai, 1994) has analyzed dispersion, non-Darcian, variable porosity and non-thermal equilibrium effects in forced convective flows through saturated porous media—which were modeled as a bed of uniform solid particles randomly packed. They concluded that the validity of the local thermal equilibrium hypothesis was strongly influenced by Darcy number, being also susceptible to the solid phase (particle) Reynolds number. As these numbers increase, local thermal equilibrium assumption looses its validity. In Sozen and Vafai (1990) the forced convective flow of a compressible fluid through a porous matrix has been studied, considering oscillating boundary conditions. An explicit finite-difference scheme was employed in the numerical

simulation, since shock waves were not present in the considered mathematical model.

Other approaches, such as theories of consolidation and multi-scales models are largely used whenever porous media deformation is accounted for. Consolidation is a time-dependent volume reduction of the soil skeleton, resulting from a load, which generates a pore-pressure distribution and, consequently, a field of relative velocities between soil particles and the liquid inside the pores. Biot (1941) formulated the first general multidimensional consolidation theory, accounting for the relation between the soil deformation and the fluid flow. The foundations of multiphase deformable porous media, employing both a generalized Biot's theory and a hybrid mixture theory (which considers both microscale and macroscale) approaches are presented in Lewis and Schrefler (1998), who discuss numerical solution methods (emphasizing finite elements) of coupled problems in porous media. Multi-scale models, in which the porous medium is treated as a system characterized by hierarchy of length scales, are largely employed in the analysis of porous media deformation. The macroscopic model is derived from an upscaling of the corresponding microscopic model, allowing deriving precise equations in the microscopic level. Besides, accurate correlation among the macroscopic parameters and the porous medium microstructure may be established. A thermomechanical model may be developed within the framework of the hybrid mixture theory (Hassanizadeh and Gray, 1980), a modification of the classical mixture theory (Atkin and Craine, 1976) in which microscopic field equations are averaged in order to identify both microscopic and macroscopic variables. In a more recent work, Hassanizadeh and Gray (1990) have developed a hybrid, thermodynamically consistent, theory to describe two-phase flow in porous media accounting for interfacial effects.

The mixture theory leads to an apparent thermomechanical independence allowing the existence of n distinct velocity fields and n distinct temperature fields (if thermal non-equilibrium is permitted), simultaneously, at each spatial point, whenever a n-constituents mixture is considered. In order to provide dynamical and thermal interactions, additional terms, absent in a Continuum Mechanics description—playing the role of momentum and energy sources—are required to account for the thermomechanical coupling among the constituents in the balance equations. Constitutive relations for these sources, satisfying the material objectivity and the Second Law of Thermodynamics, are used (Martins-Costa et al., 1992; Martins-Costa and Saldanha da Gama, 1994, 1996; Costa-Mattos et al., 1995).

Besides the momentum source, usually called a Darcian term—the cylindrical geometry gives rise to other source terms, which would be absent in a rectangular geometry, for instance. Assuming the porous matrix rigid and at rest it suffices to solve the momentum and mass balance equations for the liquid constituent. The energy balance, on the other hand, must be satisfied by the solid constituent and the liquid constituent—from now on denoted as fluid constituent. Since the gas constituent is present for allowing changes in the liquid fraction (or liquid concentration) only, no equation is required to describe its behavior.

In most cases, an accurate mathematical modeling of real problems involving transport phenomena gives rise to non-linear systems of partial differential equations. Numerical strategies to deal with these problems, such as finite element and finite difference methods, after performing a convenient discretization lead to algebraic systems of equations. In the present work a distinct approach—specifically built to deal with non-linear hyperbolic systems—is employed.

Assuming a forced convection process, a convenient numerical approach may be built in—the hydrodynamic part consisting of a non-linear hyperbolic system whose approximation is used as input for the thermal problem.

Supposing the convective flow through a cylindrical porous shell on radial direction only the hydrodynamic problem consists of a non-linear hyperbolic system of two coupled partial differential equations, whose unknowns are fluid constituent velocity and the saturation—all functions of the position and time. Like the Euler equations in gas dynamics (Chorin and Marsden, 1979), this non-linear hyperbolic system may present discontinuities—which will be shock waves in case they satisfy the entropy condition (Smoller, 1983)—in addition to classical solutions. Its numerical approximation is obtained be combining Glimm's Scheme (Glimm, 1965; Chorin, 1976)—specially designed to deal with problems with shock waves and an operator splitting technique accounting for the non-homogeneous part of the differential equations (see Martins-Costa and Saldanha da Gama, 2001 and references therein).

Most transport phenomena description involve parabolic or elliptic partial differential equations which are usually simulated by methods like finite elements, finite differences or finite volumes. Hyperbolic systems, on the other hand, allow very realistic descriptions, since the propagation of any quantity—or information—in real natural phenomena is characterized by a finite speed. However they may not admit regular solutions—requiring special tools for reliable simulations such as, for instance, Glimm's scheme or Godunov's one. Among the numerical procedures adequate to cope with discontinuous problems, Glimm's scheme is the one that better preserves the shock identity, represented by the shock magnitude and position, being a method without numerical dissipation. When compared to other numerical methodologies such as a finite element method associated with a shock capture procedure, Glimm's method presents a clear advantage of

saving computer storage memory, however its limitation to one-dimensional problems is an important shortcoming.

Glimm's scheme consists of a numerical procedure employing the solution of the associated Riemann problem to generate approximate solutions of the hyperbolic equations, when subject to arbitrary initial data. The main idea behind the method is to appropriately gather the solution of as many Riemann problems as desired to march from a time n to a time $n+1$. In short, Glimm's scheme implementation requires—for every time step, the complete solution of a Riemann problem for each two consecutive steps. In order to employ this scheme the initial data must be approximated by piecewise constant functions giving rise, for each two consecutive steps, to an initial value problem known as the Riemann problem, which must be solved for these two consecutive steps. The operator splitting technique consists of a decomposition of the hyperbolic operator in two parts so that the merely hyperbolic part of the operator—approximated by Glimm's method—is split away from its purely time evolutionary one. More specifically it consists of advancing in time through the equations representing the homogeneous problem, employing Glimm's method to obtain an initial approximation. Once this approximation has been evaluated, the numerical approximation for the solution at a successive time instant is finally reached by advancing in time to solve the purely time evolutionary problem, with the same step. These results, in turn, are used as input for the thermal problem—namely the determination of the fluid (liquid) and the solid constituents' temperatures which is simulated by means of a finite difference implicit scheme with staggered grids. Representative numerical results, showing distinct time instants to characterize the evolution in the behavior of the saturation, the fluid constituent velocity and the fluid and the solid constituents' temperatures are presented.

2. Mechanical model

2.1. Balance equations

Assuming a chemically non-reacting continuous mixture of a rigid solid constituent at rest, a liquid constituent—from now on denoted as fluid constituent and an inert gas playing the role of the third constituent, it suffices to solve mass and momentum balance equations for the fluid constituent only. It is important to emphasize that although the fluid (a liquid) is incompressible the fluid constituent is compressible, its compressibility being accounted for by the presence of an inert gas, coexisting inside the pores with the liquid. So, the mass balance is given by (Atkin and Craine, 1976; Rajagopal and Tao, 1995)

$$\frac{\partial \rho_{\mathrm{F}}}{\partial t} + \nabla \cdot (\rho_{\mathrm{F}} \mathbf{v}_{\mathrm{F}}) = 0 \tag{1}$$

in which ρ_{F} stands for the fluid constituent mass density—representing the local ratio between the fluid constituent mass and the corresponding volume of mixture and $\mathbf{v}_{\mathrm{F}}$ is the fluid constituent velocity in the mixture.

The balance of linear momentum for the fluid constituent is given by (Atkin and Craine, 1976; Rajagopal and Tao, 1995)

$$\rho_{\mathrm{F}} \left[\frac{\partial \mathbf{v}_{\mathrm{F}}}{\partial t} + (\nabla \mathbf{v}_{\mathrm{F}}) \mathbf{v}_{\mathrm{F}} \right] = \nabla \cdot \mathbf{T}_{\mathrm{F}} + \mathbf{m}_{\mathrm{F}} + \rho_{\mathrm{F}} \mathbf{b}_{\mathrm{F}} \tag{2}$$

where $\mathbf{T}_{\mathrm{F}}$ represents the partial stress tensor—analogous to Cauchy stress tensor in Continuum Mechanics—associated with the fluid constituent. The body force is represented by $\mathbf{b}_{\mathrm{F}}$ while $\mathbf{m}_{\mathrm{F}}$ is the momentum supply acting on the fluid constituent due to its interaction with the remaining constituents of the mixture. This momentum source is an internal contribution, consequently the net momentum supply to the mixture—due to all the constituents—must be zero:

$$\sum_{i=1}^{n} \mathbf{m}_i = 0 \tag{3}$$

The balance of angular momentum is satisfied through an adequate choice of $\mathbf{T}_{\mathrm{F}}$, being automatically fulfilled whenever the partial stress tensor is assumed symmetrical.

Once thermal non-equilibrium among the constituents is allowed both fluid (liquid) and solid constituents must satisfy the conservation of energy—only the gas constituent is not required to fulfill the balance equations for being an inert gas. The energy balance is given by (Atkin and Craine, 1976; Rajagopal and Tao, 1995).

$$\begin{aligned} \rho_{\mathrm{F}} c_{\mathrm{f}} \left[\frac{\partial T_{\mathrm{F}}}{\partial t} + (\nabla T_{\mathrm{F}}) \mathbf{v}_{\mathrm{F}} \right] &= -\nabla \cdot \mathbf{q}_{\mathrm{F}} + \mathbf{T}_{\mathrm{F}} \cdot D_{\mathrm{F}} + r_{\mathrm{F}} + \Pi_{\mathrm{F}} \\ \rho_{\mathrm{S}} c_{\mathrm{s}} \left[\frac{\partial T_{\mathrm{S}}}{\partial t} \right] &= -\nabla \cdot \mathbf{q}_{\mathrm{S}} + r_{\mathrm{S}} + \Pi_{\mathrm{S}} \end{aligned} \tag{4}$$

where the fluid and the solid constituents' temperatures are given, respectively, by T_{F} and T_{S}, the partial heat fluxes—analogous to the heat flux vector in Continuum Mechanics—associated with the fluid and the solid constituents by $\mathbf{q}_{\mathrm{F}}$ and $\mathbf{q}_{\mathrm{S}}$ and the external heat supplies to the fluid and the solid constituents are denoted by r_{F} and r_{S}. Also ρ_{S} represents the solid constituent mass density (the local ratio between the solid constituent mass and the corresponding volume of mixture), $\mathbf{D}_{\mathrm{F}}$ is the symmetrical part of $\nabla \mathbf{v}_{\mathrm{F}}$ tensor and c_{s} and c_{f} stand for the solid and the fluid specific heats—measured in a Continuum Mechanics context. Thermal non-equilibrium among the constituents leads to the possible existence of n distinct temperature fields at each spatial point of an n constituents' mixture—giving rise to internal heat sources—namely the fields Π_{F} and Π_{S}. More specifically,

these internal contributions Π_F and Π_S represent, respectively, the fluid constituent and the solid constituent interaction with the remaining constituents of the mixture—expressing an energy transfer per unit time and unit volume, in such a way that an n-constituents' mixture obeys the following equation (Martins-Costa et al., 1993)

$$\sum_{i=1}^{n} \Pi_i = 0 \tag{5}$$

2.2. Constitutive relations

Before presenting the constitutive relations required building a mathematical model for heat and momentum transport through rigid unsaturated porous media, an important quantity must be considered. The saturation ψ is defined as the ratio between the fluid fraction φ and the porous matrix porosity ε, so that

$$\psi = \frac{\varphi}{\varepsilon} = \frac{\rho_F}{\varepsilon \rho_f} \quad 0 \leqslant \psi \leqslant 1 \text{ everywhere} \tag{6}$$

in which ρ_f is the actual mass density of the fluid—regarded as a single continuum, in contrast to ρ_F defined as the fluid constituent mass density.

According to Williams (1978) and Saldanha da Gama and Sampaio (1987), the following constitutive relation may be considered for the momentum source term—which accounts for the dynamic interaction among the constituents, in a mixture representing an unsaturated flow of an incompressible Newtonian fluid through a porous matrix

$$\mathbf{m}_F = -\alpha \psi^2 \mathbf{v}_F - \beta \psi \nabla \psi \quad \text{with } \alpha = \frac{\varepsilon^2 \mu_f}{K}, \quad \beta = \frac{\varepsilon^2 \mu_f D}{K} \tag{7}$$

where μ_f represents the fluid viscosity (measured considering a Continuum Mechanics viewpoint), K the porous matrix specific permeability and D a diffusion coefficient—analogous to the usual mass diffusion coefficient.

An analogy with the stress tensor acting on an incompressible Newtonian fluid within a Continuum Mechanics framework probably led Williams (1978) to consider the partial stress tensor acting on the fluid constituent as being proportional to the pressure acting on it and to the gradient of its velocity. A constitutive relation analogous to the usually employed for Cauchy stress tensor with such a behavior comes as a consequence. A further simplification has been later proposed by Allen (1986), who concluded that among the three distinct momentum transfer mechanisms in the mixture—namely: shear stresses, interphase tractions and momentum transfer through fluid drag on the porous matrix, the normal fluid stresses were dominant, the shear stresses and interphase tractions being negligible when compared to the fluid drag, leading to the following approximated relation for the partial stress tensor

$$\mathbf{T}_F = -\varepsilon^2 \bar{p} \psi^2 \mathbf{I} \tag{8}$$

where $\bar{p}$ is a pressure (assumed constant while the flow is unsaturated) and $\mathbf{I}$ is the identity tensor.

A constitutive relation for the partial heat flux, analogous to the classical Fourier's law, broadly used in a Continuum Mechanics approach, is employed. These relations account for all constituents' temperatures, their thermal conductivities—measured in a Continuum Mechanics approach, being related to the material associated with each of the constituents—as well as the mixture internal structure and kinematics, being given by (see Martins-Costa and Saldanha da Gama, 1996 and references therein):

$$\begin{aligned} \mathbf{q}_F &= -\Lambda k_f \varepsilon \psi \nabla T_F \\ \mathbf{q}_S &= -\Lambda k_s (1-\varepsilon) \nabla T_S \end{aligned} \tag{9}$$

where Λ is a positive valued parameter depending on the porous medium thermal properties and internal structure and k_f and k_s represent the Newtonian fluid and the porous matrix thermal conductivities, measured in a Continuum Mechanics context. It is remarkable that, in the above stated equations the fluid constituent partial heat flux is proportional to the fluid fraction. $\varphi = \varepsilon\psi$ while the partial heat flux for the solid constituent depends on the porous matrix porosity ε.

The energy generation function Π_i is an internal contribution representing the energy supply to a given constituent arising from its thermal interaction with the remaining constituents of the mixture. The Π_i function would be zero at a given point only if the so-called thermal equilibrium assumption were assumed. Any constituent i receives energy from its interaction with the j-constituents at a higher temperature and provides energy to those at a lower temperature, according to the following constitutive relation (Costa-Mattos et al., 1995; Martins-Costa and Saldanha da Gama, 1996)

$$\Pi_i = \sum_{j=1}^{n} \hat{R}_{ij} (T_j - T_i) \tag{10}$$

The coefficient $\hat{R}_{ij}$ is a positive valued parameter that may depend on the thermal properties of j-constituents, on their velocities and on the mixture internal structure. In the mixture considered in the present work, since the gas constituent is assumed inert, thermal interaction is only present between the fluid (liquid) and the solid constituents of the mixture so that $-\Pi_S = \Pi_F$ (Martins-Costa et al., 1993) resulting in $R_{FS} = R_{SF}$ and giving rise to

$$\Pi_F = -\Pi_S = R_{FS}(T_S - T_F) \tag{11}$$

in which R_{FS} is a positive-valued factor, which depends not only on spatial position and on both constituents' thermal properties but also on their velocities, accounting for the convective heat transfer.

3. One-dimensional phenomena

The non-isothermal radial flow in the draining process of a cylindrical porous shell is now considered. Assuming all the quantities depending only on the time t and on the position r and that v is the only non-vanishing component of the fluid constituent velocity $\mathbf{v}_F$, then the balance equations (1)–(3) combined with the saturation definition (6) and the constitutive relations (7)–(11) give rise to the following set of equations:

$$\begin{aligned}
&\frac{\partial\psi}{\partial t}+\frac{\partial}{\partial r}(\psi v)=-\frac{\psi v}{r}\\
&\rho_f\varepsilon\left[\psi\frac{\partial v}{\partial t}+\psi v\frac{\partial v}{\partial r}\right]=-\frac{\partial}{\partial r}(\varepsilon^2\psi^2\bar{p})-\frac{\beta\rho_f^2\varepsilon^2}{2}\frac{\partial\psi^2}{\partial r}-\alpha\psi^2 v\\
&\varepsilon\psi\rho_f c_f\left[\frac{\partial T_F}{\partial t}+v\frac{\partial T_F}{\partial r}\right]=\Lambda k_f\varepsilon\left[\frac{1}{r}\frac{\partial}{\partial r}\left(r\psi\frac{\partial T_F}{\partial r}\right)\right]\\
&\qquad\qquad+R_{FS}\psi(T_s-T_F)\\
&(1-\varepsilon)\rho_s c_s\left[\frac{\partial T_S}{\partial t}\right]=\Lambda k_s(1-\varepsilon)\left[\frac{1}{r}\frac{\partial}{\partial r}\left(r\frac{\partial T_S}{\partial r}\right)\right]\\
&\qquad\qquad+R_{FS}\psi(T_F-T_S)
\end{aligned}\tag{12}$$

The non-linear system presented in Eq. (12) may be rewritten in a more convenient form by redefining a reference pressure p_0 as

$$p_0=\bar{p}+\frac{\beta\rho_f^2}{2}\tag{13}$$

and introducing the following dimensionless quantities:

$$\begin{aligned}
&u=v\sqrt{\frac{\rho_f}{\varepsilon p_0}},\quad \tau=\frac{t}{r_*}\sqrt{\frac{\varepsilon p_0}{\rho_f}},\quad \gamma=\frac{\alpha r_*}{\rho_f\varepsilon}\sqrt{\frac{\rho_f}{\varepsilon p_0}}\\
&\xi=\frac{r-r_i}{r_e-r_i},\quad \theta_F=\frac{T_F}{T_0},\quad \theta_S=\frac{T_S}{T_0}\\
&A_F=\frac{\Lambda k_f}{\rho_f c_f r_*}\sqrt{\frac{\rho_f}{\varepsilon p_0}},\quad B_F=\frac{R_{FS}r_*}{\varepsilon\rho_f c_f}\sqrt{\frac{\rho_f}{\varepsilon p_0}}\\
&A_S=\frac{\Lambda k_s}{\rho_s c_s r_*}\sqrt{\frac{\rho_f}{\varepsilon p_0}},\quad B_S=\frac{R_{FS}r_*}{(1-\varepsilon)\rho_s c_s}\sqrt{\frac{\rho_f}{\varepsilon p_0}}
\end{aligned}\tag{14}$$

in which $r_*=r_e-r_i$ with r_e and r_i standing for the external and internal radii of the cylindrical shell matrix and T_0 is a reference temperature. Consequently, the system presented in Eq. (12) may be rewritten as

$$\begin{aligned}
&\frac{\partial\psi}{\partial\tau}+\frac{\partial}{\partial\xi}(\psi u)=-\frac{\psi u}{\xi}\\
&\frac{\partial}{\partial\tau}(\psi u)\frac{\partial}{\partial\xi}(\psi u^2+\psi^2)=-\frac{\psi u^2}{\xi}-\gamma\psi^2 u\\
&\psi\left[\frac{\partial\theta_F}{\partial\tau}+u\frac{\partial\theta_F}{\partial\xi}\right]=\frac{A_F}{\xi}\frac{\partial}{\partial\xi}\left(\xi\psi\frac{\partial\theta_F}{\partial\xi}\right)\\
&\qquad\qquad+B_F\psi(\theta_S-\theta_F)\\
&\frac{\partial\theta_S}{\partial\tau}=\frac{A_S}{\xi}\frac{\partial}{\partial\xi}\left(\xi\frac{\partial\theta_S}{\partial\xi}\right)+B_S\psi(\theta_F-\theta_S)
\end{aligned}\tag{15}$$

4. Numerical procedure

Considering the flow not affected by the thermal problem—the usually employed forced convection assumption, a convenient procedure may be adopted. First the hydrodynamic problem stated in the first two equations of (15) is solved, its approximation being subsequently used as input for the thermal problem stated in the last two equations of (15). The numerical scheme consists in, starting from the fields, ψ, u, θ_F and θ_S at a time instant τ_n, obtain the approximations for ψ and u at a successive time τ_{n+1}. These later values are, in turn, used as input for the approximation of θ_F and θ_S at τ_{n+1}.

4.1. Hydrodynamic problem

This section presents an adequate scheme to obtain numerical approximations for the non-linear hyperbolic system of partial differential equations described in the first two equations of (15). In order to achieve this goal, two ingredients are combined: Glimm's scheme—a reliable method whose accuracy is mathematically ensured (Glimm, 1965; Chorin, 1976) and an operator splitting technique. Glimm's method is based on a theory whose mathematical formulation presents a solid thermodynamic basis—expressed by the entropy condition (Smoller, 1983). Two important features of this numerical scheme deserve a special remark. First, if the width of the steps tends to zero, the approximation obtained by Glimm's method tends to the exact solution of the problem—considering its weak formulation. Another characteristic of this scheme is that it does not dissipate shocks, preserving their magnitude (no diffusion being observed) and position.

A procedure combining an operator splitting technique (to account for the non-homogeneous portion of the differential equations) with Glimm's method has already been successfully used in other non-linear hyperbolic problems numerical simulation. Examples are wave propagation in fluids (Sod, 1977), gas flow in pipelines (Marchesin and Paes-Leme, 1983), filling-up of a porous matrix (Saldanha da Gama and Sampaio, 1987), wave propagation in a damageable elasto-viscoplastic pipe (Freitas Rachid et al., 1994), response of non-linear elastic rods (Saldanha da Gama, 1990), forced convective flow of a Newtonian fluid through an unsaturated porous slab (Saldanha da Gama and Martins-Costa, 1997) and isothermal unsaturated flow of a Newtonian fluid through a porous slab—covering most one-dimensional cases of interest (Martins-Costa and Saldanha da Gama, 2001; Martins-Costa et al., 1995). It is remarkable that the problems addressed in all these above mentioned works, due to their hyperbolic nature, do not require boundary conditions, being basically initial value problems (John, 1982).

4.2. Operator splitting technique

The operator splitting technique (see Martins-Costa and Saldanha da Gama, 2001 and references therein) is now employed in the first two equations of system (15). Essentially, this technique consists of an operator decomposition in such a way that its merely hyperbolic part—a homogeneous problem depending on both ξ and τ—is split away from its purely time evolutionary one. In other words, the original system is replaced by two problems namely the equivalent homogeneous problem and an ordinary system, whose left-hand side is a function solely of τ while its right-hand side is coincident with the original system.

Considering the original system with known initial data at a given time instant $\tau = \tau_n$, the first step to achieve its solution (ψ, u) at time $\tau = \tau_{n+1}$, consists in employing Glimm's scheme to approximate the equivalent homogeneous problem—giving rise to an initial approximation at time τ_{n+1}. In the sequence, acting in a similar way as in a prediction–correction algorithm, the following ordinary system is solved, considering the same time step $\Delta\tau = \tau_{n+1} - \tau_n$,

$$\left.\begin{aligned} &\frac{\partial \psi}{\partial \tau} = -\frac{\psi u}{\xi} \\ &\frac{\partial}{\partial \tau}(\psi u) = -\frac{\psi u^2}{\xi} - \gamma \psi^2 u \\ &\psi = \hat{\psi}_{n+1}(\xi) \\ &\psi u = (\hat{\psi}\hat{u})_{n+1}(\xi) \end{aligned}\right\} \quad \text{at } \tau = \tau_n \tag{16}$$

The system represented in the first two equations of (16) could be rewritten in a more appropriated form, by using the chain rule and substituting the first equation in the second one, as

$$\begin{aligned} &\frac{\partial \psi}{\partial \tau} = -\frac{\psi u}{\xi} \\ &\frac{\partial u}{\partial \tau} = -\gamma \psi u \end{aligned} \tag{17}$$

Assuming non-zero velocity u and non-zero saturation ψ, since no splitting would be required if either $u = 0$ or $\psi = 0$, the following ordinary equation is obtained:

$$\frac{\mathrm{d}\psi}{\mathrm{d}\tau} = -\frac{1}{\xi\gamma} \tag{18}$$

Since $1/\xi\gamma$ may be treated as a constant for a given value of ξ, Eq. (18) admits an analytical solution given by

$$\psi - \frac{1}{\xi\gamma}u = \psi_0 - \frac{1}{\xi\gamma}u_0 \Rightarrow u = \xi\gamma(\psi - \psi_0) + u_0 \tag{19}$$

in which ψ_0 and u_0 refer to information obtained at the preceding time instant by employing Glimm's method. Substituting in the first equation of (17) the expression obtained for the velocity in (19) the following analytical solution is obtained for the saturation:

$$\psi = \frac{AB\exp(A\Delta\tau)}{1+\gamma[B\exp(A\Delta\tau)]} \quad \text{with} \begin{cases} A = \psi_0\gamma - u_0/\xi \\ B = \psi_0/(A - \gamma\psi_0) \\ \Delta\tau = \tau - \tau_0 \end{cases} \tag{20}$$

Expression (20) may be substituted in (19) giving rise to an analytical solution for the velocity.

$$u = \xi\left\{-A + \gamma\frac{AB\exp(A\Delta\tau)}{1+\gamma[B\exp(A\Delta\tau)]}\right\} \text{ with} \begin{cases} A = \psi_0\gamma - u_0/\xi \\ B = \psi_0/(A - \gamma\psi_0) \\ \Delta\tau = \tau - \tau_0 \end{cases} \tag{21}$$

4.3. Glimm's scheme

Defining, by convenience, $F \equiv \psi$ and $G \equiv \psi u$, the hydrodynamic problem essentially an initial value problem subjected to a given data at τ_n may be rewritten as

$$\begin{aligned} &\frac{\partial F}{\partial \tau} + \frac{\partial G}{\partial \xi} = -\frac{G}{\xi} \\ &\frac{\partial G}{\partial \tau} + \frac{\partial}{\partial \xi}\left(\frac{G^2}{F} + F^2\right) = -\frac{G^2/F}{\xi} - \gamma F G \\ &\text{with } F = \hat{F}_n(\xi) \text{ and } G = \hat{G}_n(\xi) \quad \text{at } \tau = \tau_n \end{aligned} \tag{22}$$

in which $F = \hat{F}_n(\xi, \tau)$, and $G = \hat{G}_n(\xi, \tau)$.

Glimm's scheme is then applied to the homogeneous problem associated with (22) namely the merely hyperbolic portion of the operator given by

$$\begin{aligned} &\frac{\partial F}{\partial \tau} + \frac{\partial G}{\partial \xi} = 0 \\ &\frac{\partial G}{\partial \tau} + \frac{\partial}{\partial \xi}\left(\frac{G^2}{F} + F^2\right) = 0 \\ &F = \hat{F}_n(\xi) \quad \text{at } \tau = \tau_n \\ &G = \hat{G}_n(\xi) \quad \text{at } \tau = \tau_n \end{aligned} \tag{23}$$

This section describes the procedure to obtain a numerical approximation for the solution of the homogeneous system (22) at a time instant τ_{n+1}—denoted as $\overline{F}_{n+1}$ and $\overline{G}_{n+1}$. In order to implement Glimm's scheme, the solution of the Riemann problem associated with (23) must be previously known. Essentially, a time evolution through Glimm's scheme is performed by solving the associated Riemann problem between each two consecutive steps.

First, since the initial condition of a Riemann problem must be a step function, the arbitrary initial condition given by a function of the position ξ—namely

$$\begin{aligned} &F(\xi, 0) = F_0(\xi) \\ &G(\xi, 0) = G_0(\xi) \end{aligned} \tag{24}$$

must be approximated by piecewise constant functions. In the present work this approximation is carried out

by employing equal width steps. At a given time τ_i this approximation may be expressed as

$$\begin{aligned} F &= \hat{F}_n(\xi) \approx F_{n_i} = \hat{F}_n(\xi_i + \theta_n \Delta\xi) \\ G &= \hat{G}_n(\xi) \approx G_{n_i} = \hat{G}_n(\xi_i + \theta_n \Delta\xi) \\ &\text{for } \xi_i - \Delta\xi/2 < \xi < \xi_i + \Delta\xi/2 \end{aligned} \tag{25}$$

in which θ_n is a number randomly chosen in the open interval $(-1/2, +1/2)$ and $\Delta\xi$ is the width of each step ($\Delta\xi = \xi_{i+1} - \xi_i$).

The approximations for the initial data presented in Eq. (25) combined with the homogeneous problem presented in (23) give rise, for each two consecutive steps, to a Riemann problem (Smoller, 1983) associated with Eqs. (23).

The solution of this associated Riemann problem is the second step required implementing Glimm's scheme. In order to successively march from time $\tau = \tau_n$ to time $\tau_{n+1} = \tau_n + \Delta\tau$, the following associated Riemann problem must be solved—for each two consecutive steps

$$\begin{aligned} &\frac{\partial F}{\partial \tau} + \frac{\partial G}{\partial \xi} = 0 \\ &\frac{\partial G}{\partial \tau} + \frac{\partial}{\partial \xi}\left(\frac{G^2}{F} + F^2\right) = 0 \end{aligned} \tag{26}$$

with

$$\begin{aligned} &(F, G) = (F_{n_i}, G_{n_i}) \quad \text{for } \tau = \tau_n,\ -\infty < \xi < \xi_i + \frac{\Delta\xi}{2} \\ &(F, G) = (F_{n_{i+1}}, G_{n_{i+1}}) \quad \text{for } \tau = \tau_n,\ \xi_{i+1} - \frac{\Delta\xi}{2} < \xi < \infty \end{aligned} \tag{27}$$

The detailed solution of the Riemann problem represented by Eqs. (26) and (27) is presented in Martins-Costa and Saldanha da Gama (2001). Denoting by $\tilde{F}_{n_i}$ and $\tilde{G}_{n_i}$ the generalized solution of Eqs. (26) and (27), the approximation for the solution of Eqs. (23) at time τ_{n+1} is given as follows:

$$\begin{aligned} \overline{F}_{n+1} &= \hat{F}_{n+1}(\xi) \approx \tilde{F}_{n_i}(\xi, \tau_{n+1}) \\ \overline{G}_{n+1} &= \hat{G}_{n+1}(\xi) \approx \tilde{G}_{n_i}(\xi, \tau_{n+1}) \end{aligned} \quad \text{for } \xi_i < \xi < \xi_{i+1} \tag{28}$$

In order to prevent interactions among nearby shocks of adjacent Riemann problems, the time step $\Delta\tau$ and, consequently, τ_{n+1} must be chosen in such a way that the Courant–Friedrichs–Lewy condition (Smoller, 1983) be satisfied, thus assuring uniqueness for the solution:

$$\tau_{n+1} - \tau_n \leqslant \frac{\Delta\xi}{2|\lambda|_{\max}} \tag{29}$$

where $|\lambda|_{\max}$ is the maximum (in absolute value) propagation speed of shocks, considering all the Riemann problems at time τ_n.

At this point it is important to stress some features of Glimm's method. First if the width of the steps tends to zero the approximation obtained by Glimm's method tends to the exact solution of the problem considering its weak formulation. Another characteristic of Glimm's scheme is that it preserves shock magnitude (no diffusion being observed) and position whose admissible deviation from the correct position is of the order of magnitude of the width of each step.

After each advance in time, the obtained solution is no longer given as a step function. Thus a new random selection is required in order to build the initial condition as a step function to perform the time evolution from a given time instant τ_n to the next instant τ_{n+1} by employing Glimm's method. Once the solution for a given time instant τ_n is known, the initial data for the next step, τ_{n+1}, is approximated as

$$\begin{aligned} F_{i_n} &= F(\xi_i + \theta_n \Delta\xi, \tau_n) \\ G_{i_n} &= G(\xi_i + \theta_n \Delta\xi, \tau_n) \end{aligned} \quad \text{for } \xi_i - \frac{\Delta\xi}{2} < \xi < \xi_i + \frac{\Delta\xi}{2} \tag{30}$$

This numerical approximation of the equivalent homogeneous problem at a time instant τ_{n+1}—obtained by Glimm's scheme and denoted as $\overline{F}_{n+1}$ and $\overline{G}_{n+1}$, is combined with the solution of the ordinary system expressed by Eqs. (20) and (21), giving rise to an approximation for the solution (F, G), or, alternatively, (ψ, u), at a time instant $\tau = \tau_{n+1}$. The above-described procedure, which generates an approximation for the solution of the original system at $\tau = \tau_{n+1}$, is repeated until a specified simulation time is reached.

4.4. Thermal problem

Starting from given values for the fields F, G, θ_F and θ_S at a time instant τ_n, the previous items have described how to achieve an approximation for the solution of the hydrodynamic problem at a successive time instant $\tau = \tau_{n+1}$, given by the fields F and G. These later values are, in turn, used as input for the solution of the thermal problem namely the approximation of the dimensionless temperature fields θ_F and θ_S at τ_{n+1}. The following implicit finite difference scheme is employed to perform the thermal problem numerical approximation:

$$\begin{aligned} &F^{n+1}\left[\frac{\partial \theta_F}{\partial \tau}\right]^n + G^{n+1}\left[\frac{\partial \theta_F}{\partial \xi}\right]^n \\ &\quad = \frac{A_F}{\xi} F^{n+1}\left[\frac{\partial \theta_F}{\partial \xi}\right]^n + A_F\left[\frac{\partial F}{\partial \xi}\right]^n\left[\frac{\partial \theta_F}{\partial \xi}\right]^n \\ &\qquad + A_F F^{n+1}\left[\frac{\partial^2 \theta_F}{\partial \xi^2}\right]^n + B_F F^{n+1}[\theta_S - \theta_F]^n \\ &\left[\frac{\partial \theta_S}{\partial \tau}\right]^n = \frac{A_S}{\xi}\left[\frac{\partial \theta_S}{\partial \xi}\right]^n + A_S\left[\frac{\partial^2 \theta_S}{\partial \xi^2}\right]^n + B_S F^{n+1}[\theta_F - \theta_S]^n \end{aligned} \tag{31}$$

in which the thermal parameters A_F, B_F, A_S and B_S have been defined in Eq. (14).

5. Numerical results

The numerical procedure described in the previous sections is now illustrated through the simulation of the forced convection radial flow through the cylindrical shell porous matrix depicted in Fig. 1. The non-linear system presented in Eqs. (15) is subjected to the following initial data:

$$\left.\begin{aligned} \psi &= \hat{\psi}_0(\xi) \\ u &= \hat{u}_0(\xi) \\ \theta_F &= \hat{\theta}_{F_0}(\xi) \\ \theta_S &= \hat{\theta}_{S_0}(\xi) \end{aligned}\right\} \quad \text{for } \tau = 0 \tag{32}$$

in which the initial saturation $\hat{\psi}_0(\xi)$ has been considered either a constant value or given by distinct step functions (varying from 1 to 0.05), the initial velocity $\hat{u}_0(\xi)$ and the solid constituent initial temperature $\hat{\theta}_{S_0}(\xi)$ were assumed to be zero everywhere while for the fluid constituent initial temperature $\hat{\theta}_{F_0}(\xi)$ either a zero value or a step function (varying from 0.05 to 1), have been postulated. Besides these above described initial conditions, the system (15) observes these following boundary conditions, for $\tau > 0$:

$$\xi = 0 \Rightarrow \begin{cases} \psi = 1 \\ \partial\theta_S/\partial\xi = 0 \\ \theta_F = 0 \quad \text{or} \quad \theta_F = 1 \end{cases} \tag{33}$$

$$\xi = 1 \Rightarrow \begin{cases} \partial\theta_S/\partial\xi = 0 \\ \partial\theta_F/\partial\xi = 0 \end{cases}$$

Some selected results considering the influence of the diffusive terms' coefficients A_F and A_S, of the internal source terms' coefficients B_F and B_S as well as of the Darcian term coefficient γ are shown in Figs. 3–12. All depicted results have been obtained by employing Glimm's scheme with 300 steps for each time advance. Each considered case is presented in a set composed by six lines and four columns of graphs. Each line represents a distinct time instant—the first one being the initial condition, while each column corresponds to the behavior of a distinct variable—namely saturation, fluid

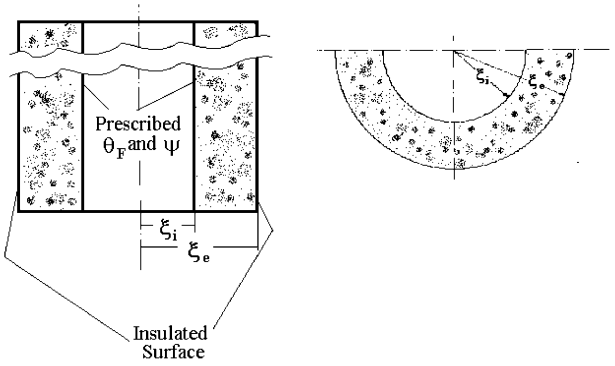

Fig. 1. Problem statement: cylindrical shell porous matrix representing a wellbore.

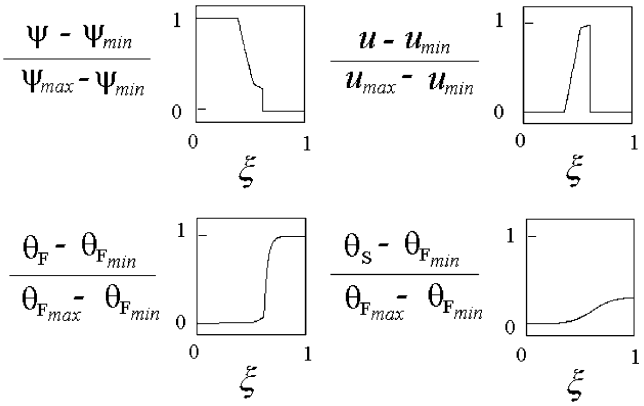

Fig. 2. Schematic diagram of the figures, representing saturation, fluid constituent velocity and fluid and solid constituents' temperatures variation with radial position for a given time instant.

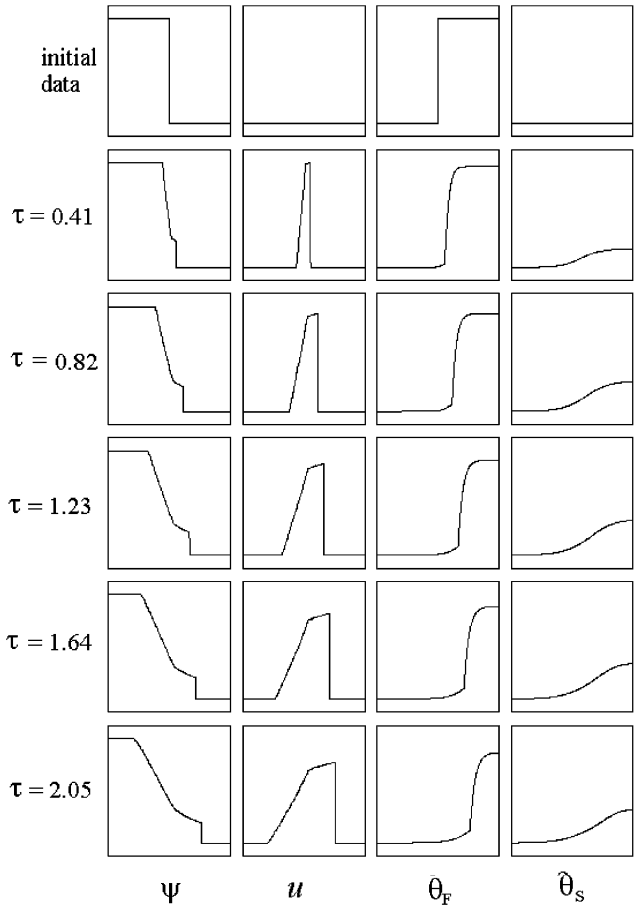

Fig. 3. Saturation, fluid constituent velocity and fluid and solid constituents' temperatures variation with radial position using $\theta_F = 0$ at ξ_i and $\theta_F = 1$ at ξ_e, with $A_F = 1$, $A_S = 10$, $B_F = 0.1$, $B_S = 10$ and $\gamma = 1$.

constituent velocity and fluid and solid constituents' temperatures. All the depicted diagrams show at the left-hand side ($\xi = 0 = \xi_i$) the cylindrical shell porous matrix internal radius, its external radius ($\xi = 1 = \xi_e$) being shown at the right-hand side. In all the depicted results the vertical axis corresponds to the numerical value assumed by, ψ, u, θ_F and θ_S, the horizontal one being the spatial coordinate ξ. Besides, all the qualitative results exhibited were obtained by employing a convenient normalization, in such a way that the minimum and maximum displayed values correspond to zero and unit values for ψ, u and θ_F, conveniently redefined as

$$\psi \to \frac{\psi - \psi_{\min}}{\psi_{\max} - \psi_{\min}}, \quad u \to \frac{u - u_{\min}}{u_{\max} - u_{\min}},$$
$$\theta_F \to \frac{\theta_F - \theta_{F\min}}{\theta_{F\max} - \theta_{F\min}} \tag{34}$$

In order that both constituents' temperatures are easily compared, θ_S is displayed using the same scale employed for θ_F, in other words,

$$\theta_S \to \frac{\theta_S - \theta_{F\min}}{\theta_{F\max} - \theta_{F\min}} \tag{35}$$

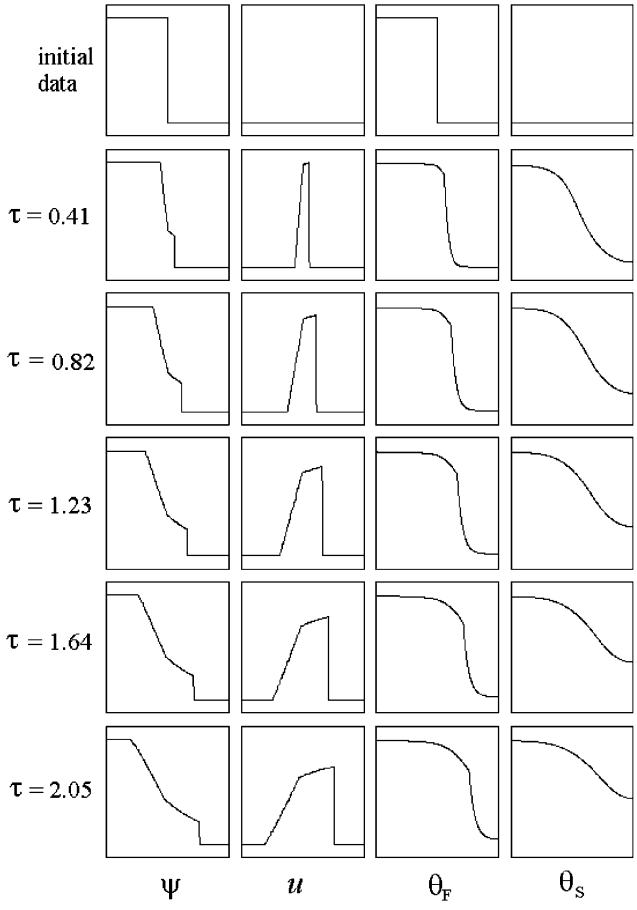

Fig. 4. Saturation, fluid constituent velocity and fluid and solid constituents' temperatures variation with radial position using $\theta_F = 1$ at ξ_i and $\theta_F = 0$ at ξ_e, with $A_F = 1$, $A_S = 10$, $B_F = 0.1$ $B_S = 10$ and $\gamma = 1$.

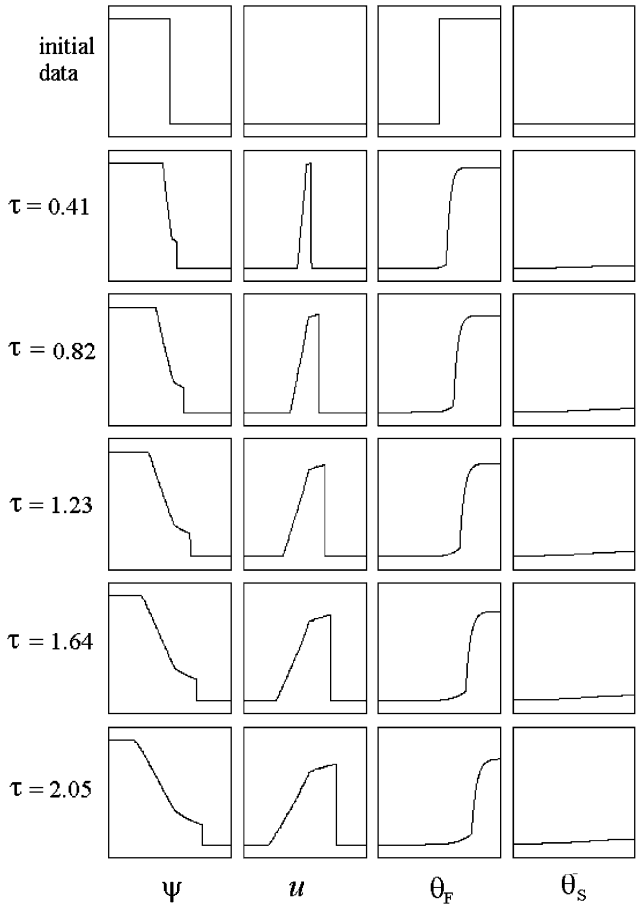

Fig. 5. Saturation, fluid constituent velocity and fluid and solid constituents' temperatures variation with radial position using $\theta_F = 0$ at ξ_i and $\theta_F = 1$ at ξ_e, with $A_F = 1$, $A_S = 10$, $B_F = 0.1$, $B_S = 1$ and $\gamma = 1$.

An important feature, present in all depicted results, is that the discontinuities for the variables ψ, u and $\partial\theta_F/\partial\xi$ are at the same spatial position, since the position of the jump for $\partial\theta_F/\partial\xi$ must be the same position for the jump of ψ. Fig. 2 presents a schematic diagram to be employed in Figs. 3–12, representing saturation, fluid constituent velocity and fluid and solid constituents' temperatures variation with radial position for a given time instant. Some conclusions, derived by considering Figs. 3–12 are now related. Initially, Fig. 3 is confronted to Figs. 4–8, through a convenient variation of A_F, A_S, B_F, B_S and γ, as well as of the initial fluid constituent temperature profile. In the sequence, again using these parameters' variation, it is possible to confront Fig. 9 to Figs. 10–12.

Figs. 3 and 4 show the influence of the fluid constituent initial temperature on the evolution of ψ, u, θ_F and θ_S. The results have been obtained by using the same values for the diffusive terms ($A_F = 1$ and $A_S = 10$), the internal heat sources ($B_F = 0.1$ and $B_S = 10$) as well as the momentum supply ($\gamma = 1$) coefficients. Also, the

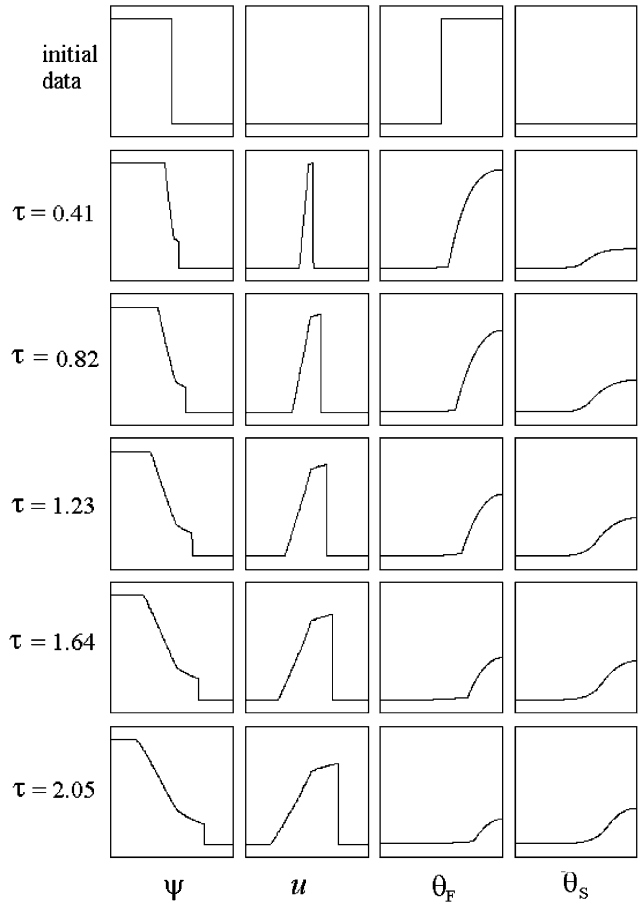

Fig. 6. Saturation, fluid constituent velocity and fluid and solid constituents' temperatures variation with radial position using $\theta_F = 0$ at ξ_i and $\theta_F = 1$ at ξ_e, with $A_F = 10$, $A_S = 1$, $B_F = 0.1$, $B_S = 10$ and $\gamma = 1$.

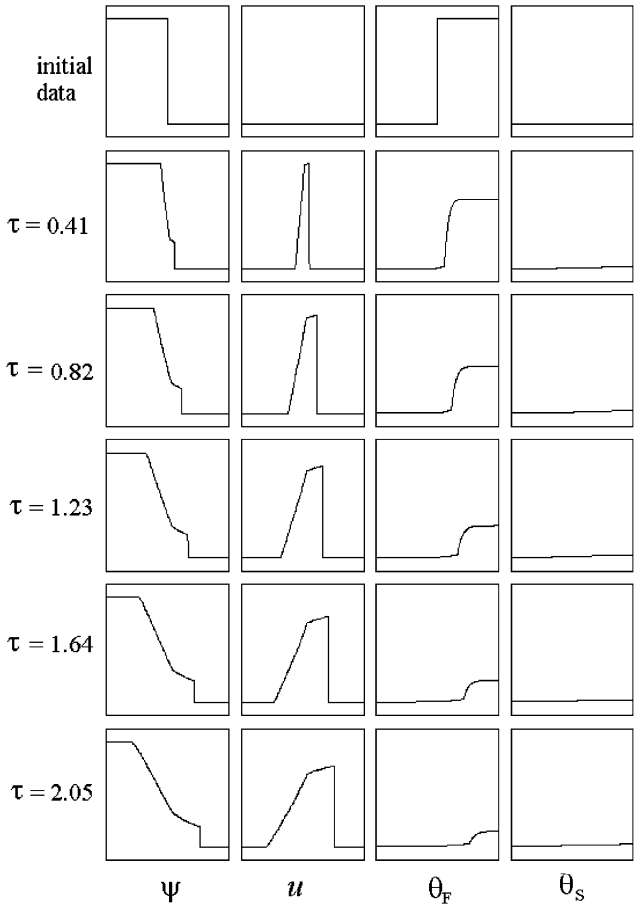

Fig. 7. Saturation, fluid constituent velocity and fluid and solid constituents' temperatures variation with radial position using $\theta_F = 0$ at ξ_i and $\theta_F = 1$ at ξ_e, with $A_F = 1$, $A_S = 10$, $B_F = 1$, $B_S = 1$ and $\gamma = 1$.

same initial data has been considered for ψ, u and θ_S, while distinct step functions describe θ_F initial behavior. In Fig. 3 the function assumes values $\theta_F = 0$ from ξ_i to an intermediate ξ and $\theta_F = 1$ from this intermediate ξ to ξ_e, and in Fig. 4 the initial temperature is given by $\theta_F = 1$ from ξ_i to ξ and $\theta_F = 0$ from ξ to ξ_e. The behavior of saturation and fluid constituent velocity remained unaltered in both cases, the variation being restricted to solid and fluid constituents' temperature profiles. The solid constituent temperature shows a more visible variation with time in Fig. 3 (given by a decay whose intensity decreases with time evolution) than in Fig. 4—the latter presenting a very discrete increase.

The influence of some coefficients present in the energy equations on the evolution of ψ, u, θ_F and θ_S may be observed by comparing Figs. 3, 5 and 6. Fig. 5 was obtained by using a solid constituent heat source coefficient ($B_S = 1$) 10 times smaller than the value employed to build Fig. 3. Comparing these two figures no variation is observed in the fluid constituent temperature, while the solid constituent profile in Fig. 5 remains almost insensitive to time evolution. An analogous behavior is observed through the confrontation of Fig. 9 (obtained with $A_F = 2$, $A_S = 10$, $B_F = 2$, $B_S = 50$ and $\gamma = 1$) and 10, in which the only varying parameter is B_F, whose value has been made 10 times greater in Fig. 10 ($B_F = 20$) than in Fig. 9, with the parameter B_S being kept constant—thus affecting both constituents' temperature profiles. The fluid constituent temperature shows a steep decay at the left-hand side while the solid constituent temperature variation along the time is barely noticed. Comparing Figs. 9 and 10 it may be seen that the increase of the parameter B_F made both solid and fluid temperature profiles almost coincident.

Comparing Figs. 3 and 6—in which both constituents diffusive term coefficients have been altered, with $A_F = 10$ (10 times greater than its value in Fig. 3) and $A_S = 1$ (10 times smaller than all previously considered values), it may be observed that the solid constituent temperature behavior remains almost unaltered. On the other hand, an important variation is observed in the fluid constituent temperature profiles.

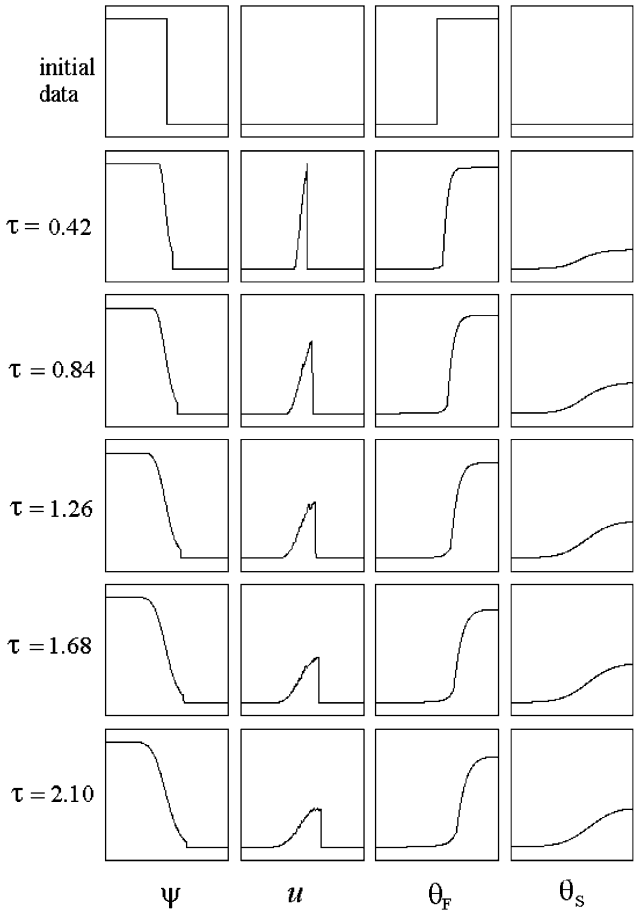

Fig. 8. Saturation, fluid constituent velocity and fluid and solid constituents' temperatures variation with radial position using $\theta_F = 0$ at ξ_i and $\theta_F = 1$ at ξ_e, with $A_F = 1$, $A_S = 10$, $B_F = 0.1$, $B_S = 10$ and $\gamma = 10$.

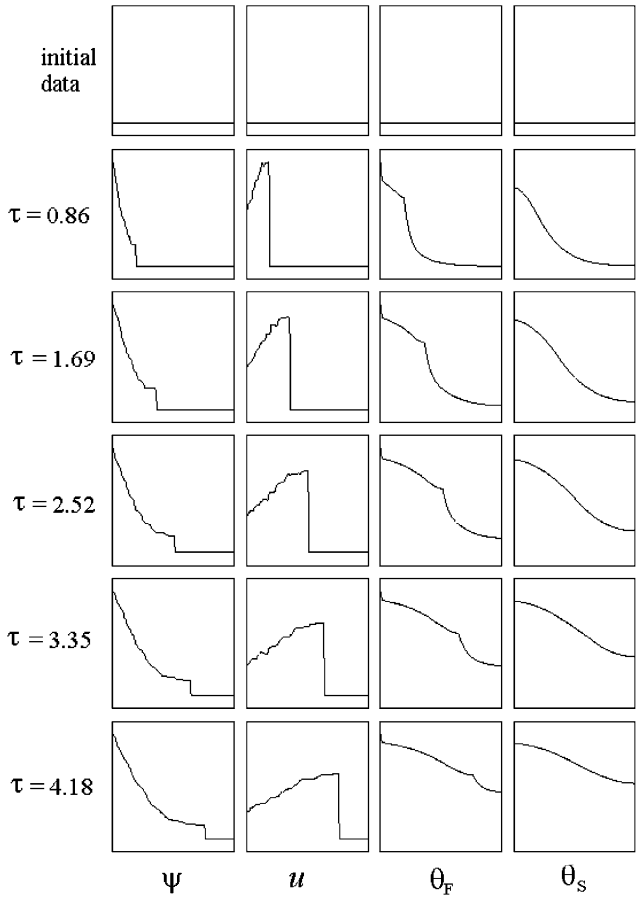

Fig. 9. Saturation, fluid constituent velocity and fluid and solid constituents' temperatures variation with radial position using $\theta_F = 0$ with $A_F = 2$, $A_S = 10$, $B_F = 2$, $B_S = 50$ and $\gamma = 1$.

The influence of the heat source coefficients in both constituents energy equations is observed by confronting Figs. 7 and 3, the former obtained considering $B_F = 1$ and $B_S = 1$, respectively 10 times greater and 10 times smaller than the values used in the latter figure. In Fig. 7, the solid constituent temperature profile shows a response almost insensitive to time evolution. On the other hand, comparing the fluid constituent behavior in the situations illustrated by these two figures, a certain "damping effect" is observed in the temperature evolution depicted in Fig. 7—when compared to Fig. 3.

In Fig. 8 the so-called Darcian term coefficient (actually the momentum source term coefficient) has been made 10 times greater ($\gamma = 10$) than all the results sketched in Figs. 3–7,—its influence on the evolution of all the considered variables being observed by confronting Figs. 3 and 8. The slight difference in the dimensionless time τ values considered for the time instants depicted in both figures—characterizing the time evolution in both problems are explained by this time evolution being related to the Courant–Friedrichs–Lewy condition expressed by Eq. (29). Comparing Figs. 8 and 3, a barely noticeable change is observed in both θ_F and θ_S profiles while a strong effect on saturation and fluid constituent velocity profiles is observed, the latter one even more pronounced—showing a kind of "damping effect" at its discontinuity. This tendency is obviously repeated by confronting Fig. 9 (considering $\gamma = 1$) and 11 (with $\gamma = 10$—also 10 times greater). A strong effect on saturation and fluid constituent velocity profiles is observed, giving rise to changes in fluid and solid constituents' temperatures. In Fig. 11 the discontinuity moves slower than in Fig. 9, the saturation shows a very steep decay and a "damping effect" on the fluid constituent velocity discontinuity may be noticed. A relatively sharp decrease at the left-hand side is also observed for the fluid constituent temperature—when compared to the profiles depicted in Fig. 9.

The effect of making the Darcian term coefficient ten times smaller ($\gamma = 0.1$) than the value employed in most depicted cases may be noticed by comparing Figs. 9 and 12. This comparison allows observing from saturation and fluid constituent velocity and temperature profiles

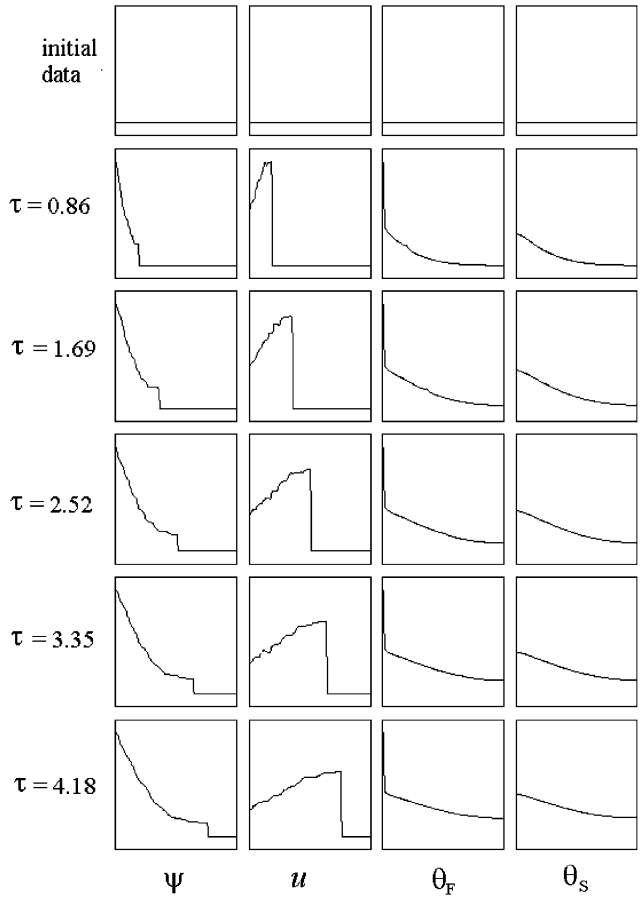

Fig. 10. Saturation, fluid constituent velocity and fluid and solid constituents' temperatures variation with radial position using $\theta_F = 0$ with $A_F = 2$, $A_S = 10$, $B_F = 20$, $B_S = 50$ and $\gamma = 1$.

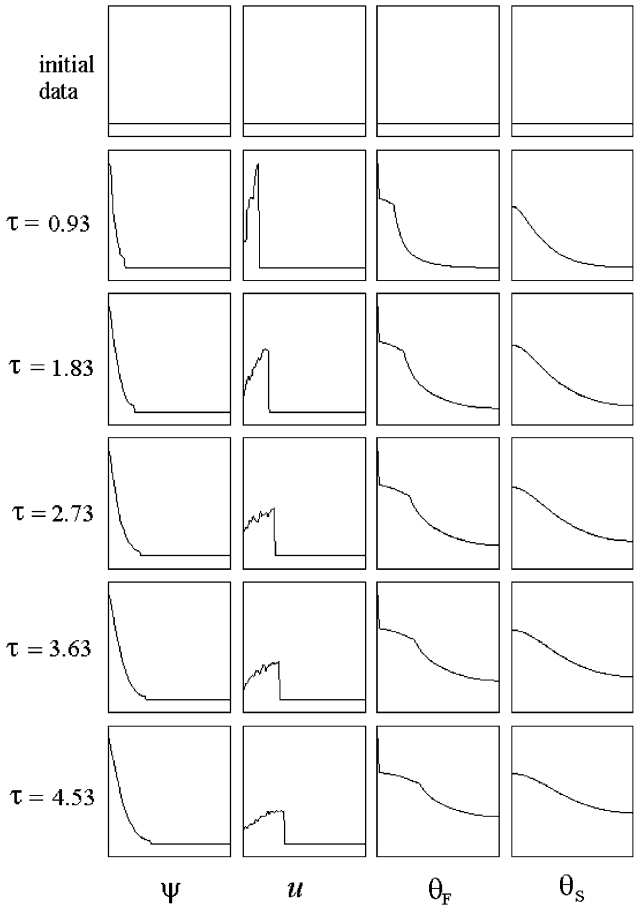

Fig. 11. Saturation, fluid constituent velocity and fluid and solid constituents' temperatures variation with radial position using $\theta_F = 0$, with $A_F = 2$, $A_S = 10$, $B_F = 2$, $B_S = 50$ and $\gamma = 10$.

that the discontinuity motion is faster in the latter than in the former. Besides, the saturation decreases quite gradually in Fig. 12 (compared to Fig. 9) and the fluid constituent temperature shows a smaller decrease at $\xi = 0$.

6. Final remarks

In this article a non-conventional numerical approach is used to study transport phenomena in an unsaturated porous matrix. Its mathematical representation gives rise to a non-linear system, whose numerical approximation is performed by first solving the hydrodynamic problem and later using the obtained solution as input for the thermal problem. The numerical methodology for approximating the hydrodynamic problem combines Glimm's scheme to an operator splitting technique—allowing the accurate approximation of a non-linear and non-homogeneous system of partial differential equations.

Glimm's method, besides preserving shock waves magnitude and position, is a convenient tool for solving one-dimensional non-linear problems, exhibiting features such as low storage costs and low computational effort, when compared to other numerical procedures to approximate non-linear problems.

The complete mathematical proof of the numerical method accuracy can be found in the works of Glimm (1965) and Chorin (1976), in which it is demonstrated that the maximum error concerning the shock position is of the order of magnitude of the step width while the shock amplitude is preserved—no shock dissipation being present.

Acknowledgments

The authors M.L. Martins-Costa and R.M. Saldanha da Gama gratefully acknowledge the financial support provided by the Brazilian agency CNPq through grants 300404/91-3 and 302462/84-8, respectively.

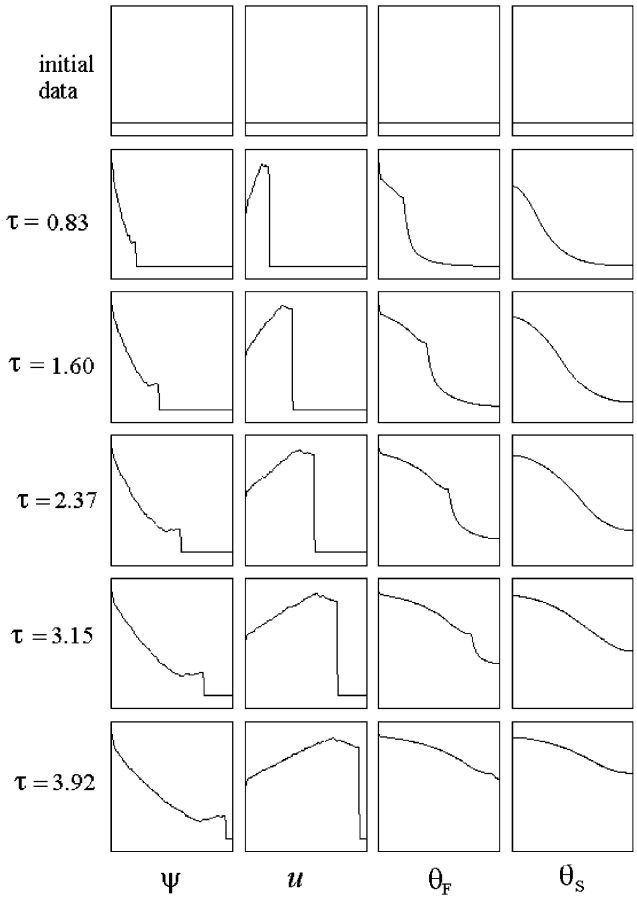

Fig. 12. Saturation, fluid constituent velocity and fluid and solid constituents' temperatures variation with radial position using $\theta_F = 0$ with $A_F = 2$, $A_S = 10$, $B_F = 2$, $B_S = 50$ and $\gamma = 0.1$.

References

Alazmi, B., Vafai, K., 2000. Analysis of variants within the porous media transport models. J. Heat Transfer 122, 303–326.

Aldouss, T.K., Jarrah, M.A., Al-Sha'erAllen, B.J., 1996. Mixed convection from a vertical cylinder embedded in a porous medium: non-Darcy model. Int. J. Heat Mass Transfer 39/6, 1141–1148.

Allen, M.B., 1986. Mechanics of multiphase fluid flows in variably saturated porous media. Int. J. Eng. Sci. 24, 339–351.

Amiri, A., Vafai, K., 1994. Analysis of dispersion effects and non-thermal equilibrium, non-Darcian, variable porosity incompressible flow through porous media. Int. J. Heat Mass Transfer 37 (6), 939–954.

Atkin, R.J., Craine, R.E., 1976. Continuum theories of mixtures. basic theory and historical development. Quart. J. Mech. Appl. Math. 29, 209–244.

Biot, M.A., 1941. General theory of three-dimensional consolidation. J. Appl. Phys. 12, 155–164.

Chang, W.J., Chang, W.L., 1996. Mixed convection in a vertical parallel-plate channel partially filled with porous media of high permeability. Int. J. Heat Mass Transfer 39/7, 1131–1342.

Chen, C.H., Chen, T.S., Chen, C.K., 1996. Non-Darcy mixed convection along nonisothermal vertical surfaces in porous media. Int. J. Heat Mass Transfer 39/6, 1157–1164.

Chorin, A.J., 1976. Random choice solution of hyperbolic systems. J. Comput. Phys. 22, 517–533.

Chorin, A.J., Marsden, J.E., 1979. A Mathematical Introduction to Fluid Mechanics. Springer-Verlag, New York.

Costa-Mattos, H., Martins-Costa, M.L., Saldanha da Gama, R.M., 1995. On the modelling of momentum and energy transfer in incompressible mixtures. Int. J. Nonlinear Mech. 30/4, 419–431.

Freitas Rachid, F.B., Saldanha da Gama, R.M., Costa-Mattos, H., 1994. Modelling the hydraulic transients in damageable elasto-viscoplastic piping systems. Appl. Math. Model. 182, 207–215.

Germain, P., Muller, P., 1986. Introduction a la Mécanique des Millieux Continus. Masson, Paris.

Glimm, J., 1965. Solutions in the large for non-linear hyperbolic systems of equations. Comm. Pure Appl. Math. 18, 697–715.

Gurtin, M.E., 1981. An Introduction to Continuum Mechanics. Academic Press, New York.

Hassanizadeh, S.M., Gray, W.G., 1980. General conservation equations for multiphase systems: 3. Constitutive theory for porous media flow. Adv. Water Resources 3, 25–40.

Hassanizadeh, S.M., Gray, W.G., 1990. Mechanics and thermodynamics of multiphase flow in porous media including interphase boundaries. Adv. Water Resources 13, 169–186.

John, F., 1982. Partial Differential Equations. Springer-Verlag, Berlin.

Lewis, R.W., Schrefler, B.A., 1998. The Finite Element Method in the Static and Dynamic Deformation and Consolidation of Porous Media. Wiley.

Marchesin, D., Paes-Leme, P.J., 1983. Shocks in gas pipelines. SIAM J. Sci. Stat. Comput. 4, 105–116.

Martins-Costa, M.L., Saldanha da Gama, R.M., 1994. A local model for the heat transfer process in two distinct flow regions. Int. J. Heat Fluid Flow 15/6, 477–485.

Martins-Costa, M.L., Saldanha da Gama, R.M., 1996. Constitutive relations for the energy transfer in nonsaturated continuous mixtures. Mech. Res. Comm. 23/2, 117–122.

Martins-Costa, M.L., Saldanha da Gama, R.M., 2001. Numerical simulation of one-dimensional flows with shock waves. Int. J. Numer. Meth. Eng. 52, 1047–1067.

Martins-Costa, M.L., Sampaio, R., Saldanha da Gama, R.M., 1992. Modelling and simulation of energy transfer in a saturated flow through a porous medium. Appl. Math. Model. 16, 589–597.

Martins-Costa, M.L., Sampaio, R., Saldanha da Gama, R.M., 1993. On the energy balance for continuous mixtures. Mech. Res. Commun. 20/1, 53–58.

Martins-Costa, M.L., Saldanha da Gama, Sampaio, R., 1995. Incompressible fluid flows through a nonsaturated porous medium. Beiträge zur Mekanik, Universität Gesamthochschule Essen, pp. 283–303.

Rajagopal, K.R., Tao, L., 1995. Mechanics of MixturesSeries on Advances in Mathematics for Applied Sciences, vol. 35. World Scientific, Singapore.

Saldanha da Gama, R.M., 1990. An alternative procedure for simulating the dynamical response of non-linear elastic rods. Int. J. Numer. Meth. Eng. 29, 123–139.

Saldanha da Gama, R.M., Martins-Costa, M.L., 1997. Numerical simulation of transport phenomena in nonsaturated porous media. In: ASME Proceedings of the 32nd National Heat Transfer Conference, HTD-vol. 339, Baltimore, USA, pp. 99–106.

Saldanha da Gama, R.M., Sampaio, R., 1987. A model for the flow of an incompressible Newtonian fluid through a nonsaturated infinite rigid porous medium. Comput. Appl. Math. 6/2, 195–205.

Smoller, J., 1983. Shock Waves and Reaction-Diffusion Equations. Springer-Verlag, New York.

Sod, G.A., 1977. Numerical study of a converging cylindrical shock. J. Fluid Mech. 83, 785–794.

Sozen, M., Vafai, K., 1990. Analysis of oscillating compressible flow through a packed bed. Int. J. Heat Fluid Flow 12, 130–138.

Tien, C.L., Vafai, K., 1990. Simultaneous heat and mass transfer accompanied by phase change in porous insulation. Adv. Appl. Mech. 27, 132–140.

Truesdell, C., 1957. Sulle Basi della Termomeccanica. Rendiconnti Accademia Lincei Ser. 8/22, 33–38, and pp. 158–166.

Vafai, K., Whitaker, S., 1986. Simultaneous heat and mass transfer accompanied by phase change in porous insulation. J. Heat Transfer 108, 225–281.

Williams, W.O., 1978. Constitutive equations for a flow of an incompressible viscous fluid through a porous medium. J. Heat Transfer 36, 255–267.